Effect of pressure on the crystal structure of L-serine-I and the crystal structure of L-serine-II at 5.4 GPa

Acta Crystallographica Section B
Structural Science
ISSN 0108-7681

Effect of pressure on the crystal structure of L-serine-I and the crystal structure of L-serine-II at 5.4 GPa

Stephen A. Moggach,[a] David R. Allan,[a] Carole A. Morrison,[a] Simon Parsons[a]* and Lindsay Sawyer[b]

[a]School of Chemistry and Centre for Science at Extreme Conditions, The University of Edinburgh, King's Buildings, West Mains Road, Edinburgh EH9 3JJ, Scotland, and [b]Institute for Cell and Molecular Biology and Centre for Science at Extreme Conditions, The University of Edinburgh, King's Buildings, West Mains Road, Edinburgh EH9 3JR, Scotland

Correspondence e-mail: s.parsons@ed.ac.uk

Received 2 August 2004
Accepted 30 November 2004

The crystal structure of L-serine has been determined at room temperature at pressures between 0.3 and 4.8 GPa. The structure of this phase (hereafter termed L-serine-I), which consists of the molecules in their zwitterionic tautomer, is orthorhombic, space group $P2_12_12_1$. The least compressible cell dimension (c), corresponds to chains of head-to-tail NH$\cdots$carboxylate hydrogen bonds. The most compressible direction is along **b**, and the pressure-induced distortion in this direction takes the form of closing up voids in the middle of R-type hydrogen-bonded ring motifs. This occurs by a change in the geometry of hydrogen-bonded chains connecting the hydroxyl groups of the $-CH_2OH$ side chains. These hydrogen bonds are the longest conventional hydrogen bonds in the system at ambient pressure, having an O$\cdots$O separation of 2.918 (4) Å and an O$\cdots$O$\cdots$O angle of 148.5 (2)°; at 4.8 GPa these parameters are 2.781 (11) and 158.5 (7)°. Elsewhere in the structure one NH$\cdots$O interaction reaches an N$\cdots$O separation of 2.691 (13) Å at 4.8 GPa. This is amongst the shortest of this type of interaction to have been observed in an amino acid crystal structure. Above 4.8 GPa the structure undergoes a single-crystal-to-single-crystal phase transition to a hitherto uncharacterized polymorph, which we designate L-serine-II. The OH$\cdots$OH hydrogen-bonded chains of L-serine-I are replaced in L-serine-II by shorter OH$\cdots$carboxyl interactions, which have an O$\cdots$O separation of 2.62 (2) Å. This phase transition occurs *via* a change from a *gauche* to an *anti* conformation of the OH group, and a change in the $NC_\alpha CO$ torsion angle from $-178.1\ (2)^\circ$ at 4.8 GPa to $-156.3\ (10)^\circ$ at 5.4 GPa. Thus, the same topology appears in both crystal forms, which explains why it occurs from one single-crystal form to another. The transition to L-serine-II is also characterized by the closing-up of voids which occur in the centres of other R-type motifs elsewhere in the structure. There is a marked increase in CH$\cdots$O hydrogen bonding in both phases relative to L-serine-I at ambient pressure.

1. Introduction

Molecular crystals display a wide range of intermolecular interactions, from strong ionic and hydrogen-bonding contacts to weak van der Waals contacts. The application of high pressure to organic materials is a very powerful way to probe the nature of these interactions. The magnitudes of the effects which are observed are generally greater than those observed on cooling. Pressure-induced polymorphism occurs in a number of systems. We have characterized, for example, new high-pressure phases in alcohols (Allan & Clark, 1999; Allan *et al.*, 2001, 2002), carboxylic acids (Allan *et al.*, 1998, 2000),

acetone (Allan *et al.*, 1999) and, very recently, glycine (Dawson *et al.*, 2005). A different high-pressure phase of glycine has also been recently reported by Boldyreva *et al.* (2004). The number of high-pressure studies on molecular systems that have actually been carried out is still rather small and systematic trends have yet to emerge. However, this is a rapidly emerging area of structural science and it has been the subject of a number of recent reviews, for example, Boldyreva (2003, 2004*a*,*b*,*c*), Katrusiak (2004) and Hemley & Dera (2000).

Organic compounds crystallize predominantly in low-symmetry crystal systems and the effect of the application of pressure is generally quite anisotropic. The compressibility along different crystallographic directions can occasionally be rationalized in terms of the strengths of hydrogen bonds made along different directions. For example, both Boldyreva *et al.* (2003) and we (Dawson *et al.*, 2005) have shown that the least compressible lattice direction of α-glycine corresponds to the direction of strongly hydrogen-bonded chains. However, in $[Co(NH_3)_5NO_2]Cl_2$ some hydrogen bond lengths actually increase with pressure (Boldyreva *et al.*, 1998) and it is clear that the behaviour of hydrogen bonds under high pressure depends not only on the bonds themselves, but also on their relationship to other features of a structure, such as other intermolecular interactions and crystal packing.

The extent to which compressibility can be explained, and how far a structure can be compressed before it undergoes a phase transition, are key issues of current interest in this area of crystallography. In this paper we attempt to address them in a study of the effect of pressure on L-serine. Amino acids have been studied extensively at ambient pressure both by neutron and X-ray diffraction; they are highly crystalline and their structures are dominated by hydrogen bonding (Jeffrey & Maluszynska, 1982). Weak CH$\cdots$O hydrogen bonds occur frequently and play an important role in supporting more familiar medium-strength hydrogen bonds, *e.g.* NH$\cdots$O (Desiraju & Steiner, 1999; Derewenda *et al.*, 1995). Amino acids therefore make excellent candidates for this kind of study, but we hope that the results will additionally be useful for the development of inter-residue potentials which can be used to model the nature of pressure effects in proteins and other complex systems.

2. Experimental

2.1. Crystal growth

L-Serine (99%) was purchased from Aldrich (catalogue number S2,60-0). One small, block-shaped crystal was obtained directly from the sample bottle and loaded into a diamond anvil cell.

2.2. High-pressure crystallography

High-pressure experiments were carried out using a Merrill–Bassett diamond anvil cell (half-opening angle 40°), equipped with brilliant-cut diamonds with 600 µm culets and a tungsten gasket (Merrill & Bassett, 1974). A 1:1 mixture of *n*-pentane and isopentane was used as a hydrostatic medium. A small ruby chip was also loaded into the cell as the pressure calibrant, with the ruby fluorescence method utilized to measure the pressure. Measurements were carried out by excitation with a 632.417 nm line from a He–Ne laser, the fluorescence being detected with a Jobin–Yvon LabRam 300 Raman spectrometer.

Diffraction data were collected on a Bruker SMART APEX diffractometer with graphite-monochromated Mo $K\alpha$ radiation (λ = 0.71073 Å). A hemisphere of data was collected at room temperature using the crystal before it was mounted in the Merrill–Bassett cell. The crystal was orthorhombic and its unit-cell dimensions were a = 8.579 (4), b = 9.349 (4), c = 5.613 (3) Å based on 783 data $8 < 2\theta < 45°$. The L-serine coordinates of Kistenmacher *et al.* (1974) were refined against these data to yield a conventional R-factor of 0.029 for 408 data with $I > 2\sigma(I)$. The aim of this experiment was simply to establish the starting phase of the sample used in this pressure study, and further crystallographic data are not given here.

Data collection and processing procedures for the high-pressure experiments were as described by Dawson *et al.* (2004). Integrations were carried out using the program *SAINT* (Bruker AXS, 2003), and absorption corrections with the programs *SADABS* (Sheldrick, 2004) and *SHADE* (Parsons, 2004). Data collections were taken in approximately 1.0 GPa steps from 0.3 GPa up to a final pressure of 5.4 GPa. Determinations of the cell constants at 5.4 GPa showed that a single-crystal-to-single-crystal phase transition had occurred to a new polymorph (L-serine-II). The pressure was then reduced back down to ambient pressure and the sample removed from the pressure cell. Once removed, a hemisphere of X-ray diffraction data was collected at room temperature. The phase on return to ambient pressure was identified as L-serine-I on the basis of the unit-cell constants [orthorhombic, a = 8.531 (9), b = 9.249 (10), c = 5.581 (6) Å] and structure refinement of L-serine-I coordinates yielded a conventional R factor of 0.041. This experiment aimed simply to establish the phase of serine after removal from the cell so further data are not given here.

Refinements of the compressed form of L-serine-I were carried out starting from the published coordinates determined at ambient pressure. The structure of the new phase (L-serine-II) was solved by the global minimization method using the program *DASH* (David *et al.*, 2001). Refinements were carried out against $|F|^2$ using all data (*CRYSTALS*; Betteridge *et al.*, 2003). Owing to the low completeness of the data sets, all 1,2 and 1,3 distances were restrained to the values observed in the ambient pressure structure, and all C, N and O atoms were refined with isotropic displacement parameters.

H atoms attached to carbon and nitrogen were placed geometrically and not refined. At ambient pressure Kistenmacher *et al.* (1974) showed that the hydroxyl H atom (H7) eclipses C3—H2 with r(OH) = 0.88 Å and <COH = 107°; we have confirmed these results. This feature is ascribable to the formation of intermolecular OH$\cdots$OH hydrogen bonds (see §3). In placing the hydroxyl H atom (H7) in the structures between 0.3 and 4.8 GPa, we initially assumed that the

Table 1
Crystallographic data for L-serine at increasing pressures.

Weighting scheme: $p = P(6)*\max(F_o^2,0) + (1 - P(6))F_c^2$. Method = *SHELXL*97 (Sheldrick, 1997).

Pressure	0.3 GPa	1.4 GPa	2.9 GPa
Crystal data			
Chemical formula	$C_3H_7NO_3$	$C_3H_7NO_3$	$C_3H_7NO_3$
M_r	105.09	105.09	105.09
Cell setting, space group	Orthorhombic, $P2_12_12_1$	Orthorhombic, $P2_12_12_1$	Orthorhombic, $P2_12_12_1$
a, b, c (Å)	8.5213 (13), 9.172 (2), 5.5847 (8)	8.4365 (10), 8.9506 (19), 5.5512 (6)	8.3702 (10), 8.7699 (19), 5.5103 (6)
V (Å^3)	436.47 (15)	419.18 (11)	404.49 (11)
Z	4	4	4
D_x (Mg m^{-3})	1.599	1.665	1.726
Radiation type	Mo $K\alpha$	Mo $K\alpha$	Mo $K\alpha$
No. of reflections for cell parameters	246	270	258
θ range (°)	9–46	9–46	9–47
μ (mm^{-1})	0.14	0.15	0.15
Temperature (K)	293	293	293
Crystal form, colour	Block, colourless	Block, colourless	Block, colourless
Crystal size (mm)	0.20 × 0.10 × 0.10	0.20 × 0.10 × 0.10	0.20 × 0.10 × 0.10
Data collection			
Diffractometer	Bruker SMART	Bruker SMART	Bruker SMART
Data collection method	ω scans	ω scans	ω scans
Absorption correction	Multi-scan (based on symmetry-related measurements)	Multi-scan (based on symmetry-related measurements)	Multi-scan (based on symmetry-related measurements)
T_{min}	0.695	0.552	0.711
T_{max}	1.00	1.00	1.00
No. of measured, independent and observed reflections	1169, 151, 93	1006, 146, 100	1112, 134, 100
Criterion for observed reflections	$I > 2\sigma(I)$	$I > 2\sigma(I)$	$I > 2\sigma(I)$
R_{int}	0.138	0.127	0.119
θ_{max} (°)	23.1	23.3	23.3
Range of h, k, l	$-9 \Rightarrow h \Rightarrow 9$ $-3 \Rightarrow k \Rightarrow 3$ $-6 \Rightarrow l \Rightarrow 6$	$-9 \Rightarrow h \Rightarrow 9$ $-3 \Rightarrow k \Rightarrow 3$ $-6 \Rightarrow l \Rightarrow 6$	$-9 \Rightarrow h \Rightarrow 9$ $-3 \Rightarrow k \Rightarrow 3$ $-6 \Rightarrow l \Rightarrow 6$
Refinement			
Refinement on	F^2	F^2	F^2
$R[F^2 > 2\sigma(F^2)]$, $wR(F^2)$, S	0.083, 0.214, 1.07	0.073, 0.164, 1.14	0.065, 0.154, 1.07
No. of reflections	140	135	133
No. of parameters	33	33	33
H-atom treatment	Mixture of independent and constrained refinement	Mixture of independent and constrained refinement	Mixture of independent and constrained refinement
Weighting scheme	$w = 1/[\sigma^2(F^2) + (P(1)p)^2 + P(2)p + P(4) + P(5)\sin\theta]$; $P(i)$ are: $0.909E^{-1}$, 2.37, 0.00, 0.00, 0.00, 0.333	$w = 1/[\sigma^2(F^2) + (P(1)p)^2 + P(2)p + P(4) + P(5)\sin\theta]$; $P(i)$ are: $0.291E^{-1}$, 2.72, 0.00, 0.00, 0.00, 0.333	$w = 1/[\sigma^2(F^2) + (P(1)p)^2 + P(2)p + P(4) + P(5)\sin\theta]$; $P(i)$ are: $0.597E_{-1}$, 1.46, 0.00, 0.00, 0.00, 0.333
$(\Delta/\sigma)_{max}$	<0.0001	<0.0001	<0.0001
$\Delta\rho_{max}$, $\Delta\rho_{min}$ (e Å^{-3})	0.30, −0.23	0.37, −0.27	0.26, −0.24
Extinction method	Larson (1970)	Larson (1970)	Larson (1970)
Extinction coefficient	60 (50)	30 (20)	30 (30)

	4.1 GPa	4.8 GPa	5.4 GPa
Crystal data			
Chemical formula	$C_3H_7NO_3$	$C_3H_7NO_3$	$C_3H_7NO_3$
M_r	105.09	105.09	105.09
Cell setting, space group	Orthorhombic, $P2_12_12_1$	Orthorhombic, $P2_12_12_1$	Orthorhombic, $P2_12_12_1$
a, b, c (Å)	8.3266 (13), 8.665 (3), 5.4851 (8)	8.2980 (16), 8.600 (3), 5.4663 (10)	6.9083 (10), 9.644 (3), 5.6166 (8)
V (Å^3)	395.75 (15)	390.09 (17)	374.19 (14)
Z	4	4	4
D_x (Mg m^{-3})	1.764	1.789	1.865
Radiation type	Mo $K\alpha$	Mo $K\alpha$	Mo $K\alpha$
No. of reflections for cell parameters	258	247	313
θ range (°)	9–47	9–44	6–46
μ (mm^{-1})	0.16	0.16	0.17
Temperature (K)	293	293	293
Crystal form, colour	Block, colourless	Block, colourless	Block, colourless
Crystal size (mm)	0.20 × 0.10 × 0.10	0.20 × 0.10 × 0.10	0.20 × 0.10 × 0.10
Data collection			
Diffractometer	Bruker SMART	Bruker SMART	Bruker SMART

Table 1 (continued)

	4.1 GPa	4.8 GPa	5.4 GPa
Data collection method	ω scans	ω scans	ω scans
Absorption correction	Multi-scan (based on symmetry-related measurements)	Multi-scan (based on symmetry-related measurements)	Multi-scan (based on symmetry-related measurements)
T_{min}	0.721	0.739	0.687
T_{max}	1.00	1.00	1.00
No. of measured, independent and observed reflections	1112, 130, 103	1068, 129, 99	1990, 140, 90
Criterion for observed reflections	$I > 2\sigma(I)$	$I > 2\sigma(I)$	$I > 2\sigma(I)$
R_{int}	0.080	0.083	0.081
θ_{max} (°)	23.4	23.2	23.3
Range of h, k, l	$-9 \Rightarrow h \Rightarrow 9$ $-2 \Rightarrow k \Rightarrow 2$ $-6 \Rightarrow l \Rightarrow 6$	$-9 \Rightarrow h \Rightarrow 9$ $-2 \Rightarrow k \Rightarrow 2$ $-6 \Rightarrow l \Rightarrow 6$	$-7 \Rightarrow h \Rightarrow 7$ $-3 \Rightarrow k \Rightarrow 3$ $-6 \Rightarrow l \Rightarrow 6$
Refinement			
Refinement on	F^2	F^2	F^2
$R[F^2 > 2\sigma(F^2)]$, $wR(F^2)$, S	0.066, 0.165, 1.06	0.060, 0.122, 1.15	0.048, 0.102, 1.21
No. of reflections	129	128	121
No. of parameters	32	33	32
H-atom treatment	Mixture of independent and constrained refinement	Mixture of independent and constrained refinement	Mixture of independent and constrained refinement
Weighting scheme	$w = 1/[\sigma^2(F^2) + (P(1)p)^2 + P(2)p + P(4) + P(5)\sin\theta]$; $P(i)$ are: $0.672E^{-1}$, 1.89, 0.00, 0.00, 0.00, 0.333	$w = 1/[\sigma^2(F^2) + (P(1)p)^2 + P(2)p + P(4) + P(5)\sin\theta]$; $P(i)$ are: 0.00, 1.64, 0.00, 0.00, 0.00, 0.333	$W = 1/[\sigma^2(F^2) + (P(1)p)^2 + P(2)p + P(4) + P(5)\sin\theta]$ $P(i)$ are: $0.219E^{-1}$, 1.16, 0.00, 0.00, 0.00, 0.333
$(\Delta/\sigma)_{max}$	<0.0001	<0.0001	<0.0001
$\Delta\rho_{max}$, $\Delta\rho_{min}$ (e Å^{-3})	0.25, −0.20	0.19, −0.21	0.25, −0.20
Extinction method	None	Larson (1970)	None
Extinction coefficient	–	44 (19)	–

ambient pressure conformation of the CH_2OH side chain was retained and this atom was placed in an ideal position for OH···OH hydrogen bonding. However, the positional parameters of H7 were refined subject to the restraints r(O—H) = 0.88 (1) Å and < COH = 107 (1)°, so enabling the HOCC torsion angle to optimize. In all except the 4.8 GPa data set O3—H7 eclipsed C2—H2 as it does at ambient pressure. At 4.8 GPa O3—H7 appeared to adopt a staggered orientation with respect to the neighbouring CH_2 group; refinements in which it was restrained in an eclipsed position failed to converge. Of course, the standard uncertainties on the positional parameters of H7 are so large that the differences between the two models are not statistically significant, but in the 4.8 GPa model presented here H7 is left in its refined position. A definitive statement regarding the position of H7 at 4.8 GPa is not possible from these data, but neutron diffraction experiments would clarify this issue. At 5.4 GPa, H7 was observed in a difference map, but treated during refinement in the same way as at lower pressure. All distances and angles involving H quoted in this paper were calculated after normalizing the H-atom position to mimic those that might be obtained by neutron diffraction [r(C—H) = 1.083, r(N—H) = 1.009, r(O—H) = 0.983 Å].

Listings of crystal and refinement data are given in Table 1.[1]

Crystal structures were visualized using the programs *CAMERON* (Watkin *et al.*, 1993) and *MERCURY* (Bruno *et al.*, 2002). Analyses were carried out using *PLATON* (Spek, 2004), as incorporated in the *WIN-GX* suite (Farrugia, 1999). Searches of the Cambridge Database (Allen, 2002; Allen & Motherwell, 2002) utilized the program *CONQUEST* and Version 5.25 of the database with updates up to April 2004.

The numbering scheme used is the same as in the CSD refcode LSERIN01 (Kistenmacher *et al.*, 1974). In macromolecular structures our C2, C3 and O3 would be designated C*A*, C*B* and O*G*, respectively. The settings of the structures reported here are the same as used in LSERIN01; that used for L-serine-II was chosen to facilitate the comparison with L-serine-I.

3. Results and discussion

3.1. Structure of L-serine-I at ambient pressure

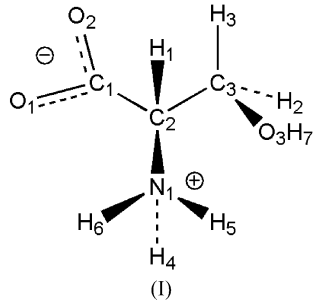

(I)

Prior to this work there was only one known crystalline form of anhydrous L-serine and this crystallizes with one molecule

[1] Supplementary data for this paper are available from the IUCr electronic archives (Reference: WS5017). Services for accessing these data are described at the back of the journal.

in the asymmetric unit in the space group $P2_12_12_1$. We refer to this form as L-serine-I. The structure was determined using X-ray diffraction by Benedetti *et al.* (1973) and then later by Kistenmacher *et al.* (1974). The serine molecule is in its zwitterionic form [see (I)], with the CH_2OH side-chain in the *gauche* conformation with respect to the ammonium and carboxyl groups ($\chi_1 = 61.5^\circ$). This conformation is observed under all conditions investigated during this work.

The structure of L-serine-I is dominated by hydrogen bonding (Figs. 1*a*–3*a* show projections of the structure along **a**, **b** and **c**, respectively). Many amino-acid crystal structures have one cell dimension of *ca* 5.5 Å and this is associated with a head-to-tail chain motif formed by NH···OOC interactions. This is observed in L-serine-I, where the molecules form a chain *via* lattice repeats along the crystallographic *c* direction through three-centre N1H5···O1/2 interactions (Fig. 1*a*). Jeffrey & Maluszynska (1982) have shown that such interactions can take on varying degrees of asymmetry and that observed here is relatively symmetrical, with distances of 1.91 (H5···O2) and 2.29 Å (H5···O1). If the weaker hydrogen bond is ignored, the graph-set descriptor of this chain is $C(5)$ (Bernstein *et al.*, 1995).

A second $C(5)$ chain, generated by the 2_1 about **c**, is linked to the first *via* N1H6···O1 hydrogen bonds [N1···O1 2.840 (4) Å)] to form a ribbon. The N1H6···O1 interactions also generate primary level $C(5)$ chains along the ribbon. Along the length of the ribbon the combination of the two $C(5)$ chains forms secondary-level $R_3^3(11)$ ring motifs. The CH_2OH side chains are distributed along the outside edges of the ribbons and these interact *via* C(2)···O3H7···O3H7 hydrogen bonds to link the ribbons into layers. The hydrogen bonds between the hydroxyl groups are quite weak, with O3···O3 measuring 2.918 (4) Å under ambient conditions. The combination of the $C(2)$ and $C(5)$ N1H5 . . . . ···O2 chains generates secondary-level $R_3^3(13)$ ring motifs (Fig. 1*a*).

The layers are stacked along **a**, having a sinusoidal appearance when viewed in projection onto (001) (Fig. 3*a*). The layers are linked by N1H4···O2 interactions which form yet another primary level $C(5)$ chain which runs along **a** (Fig. 2*a*). The intersection of the N1H5···O2 and N1H4···O2 $C(5)$ chains along **a** and **c** builds a third set of secondary-level ring motifs, these having the descriptor $R_4^3(14)$.

The N1H5···O2 and N1H4···O2 interactions actually build another layer which is parallel to the *ac* plane (Fig. 2*a*). Overall then, the structure consists of two sets of layers: one stacks along **a** and contains $R_3^3(11)$ and $R_3^3(13)$ ring motifs, the other is more planar, stacks along **b** and contains $R_4^3(14)$ rings. We shall refer to these as the *A* and *B* layers, respectively. The N1H4···O2 interactions which occur within the *B* layers can also be viewed as interactions between the *A* layers; similarly, the N1H6···O1 and O3H7···O3H7 interactions within the *A* layers serve to link the *B* layers (Fig. 3*a*). The N1H5···O2 hydrogen bonds are common to both layers.

Plots of the cell dimensions and volume of L-serine as a function of pressure are given in Fig. 4. L-Serine-I is stable to 4.8 GPa (48 kbar). Above this pressure it undergoes a single-crystal-to-single-crystal phase transition to a new phase, which we designate L-serine-II. We prefer this I-, II-, *etc.* phase nomenclature to the α-, β-, *etc.* nomenclature for amino acids even though the polymorphs of glycine are denoted α, β, γ,

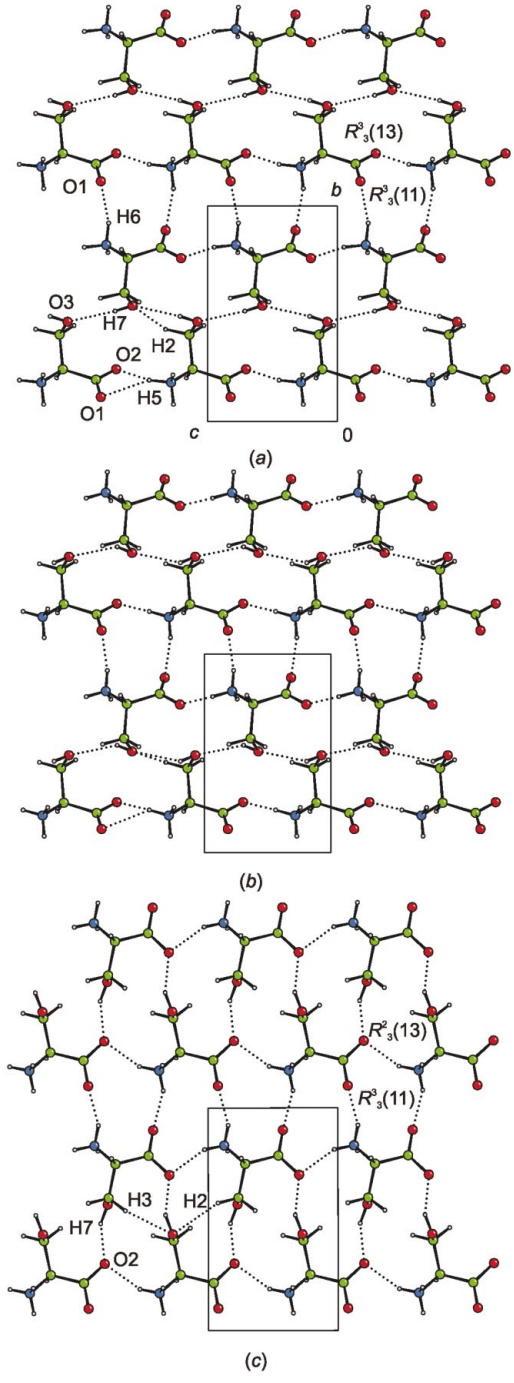

Figure 1
Effect of pressure on the crystal structure of L-serine as viewed along **a**: (*a*) L-serine-I at ambient pressure; (*b*) L-serine-I at 4.8 GPa; (*c*) L-serine-II at 5.4 GPa. This layer is referred to as the *A*-layer in the text. Colour scheme: red oxygen, blue nitrogen, green carbon and white hydrogen. The orientations of all diagrams are the same; the scale is the same as that used in Figs. 2 and 3. The bifurcation of the N1H5···O1/2 and CH···O bonding are shown only in the bottom-left fragment of the diagram.

etc. because the symbols α and β are used for other purposes in amino-acid chemistry.

3.2. Response of L-serine-I to pressure up to 4.8 GPa

The response of the unit-cell dimensions of L-serine-I to high pressure is anisotropic (Fig. 4), although, since the crystal system is orthorhombic, the principal axes of the strain tensor must be coincident with the crystallographic axes. The largest reduction occurs in the *b* axis (6.2%), while the *a* and *c* axes change by 2.6 and 2.1%, respectively. The volume changes most rapidly between 0.2 and 2.9 GPa, and then the trend flattens-off up to 4.8 GPa; above 4.8 GPa all three axis lengths change suddenly during the transition to L-serine-II. Fig. 5 shows the superposition of the structures of L-serine-I at ambient pressure and at 4.8 GPa, where the molecules are represented by their inertial tensors. The orientations of the molecules change slightly, but the large compression along **b** is readily apparent.

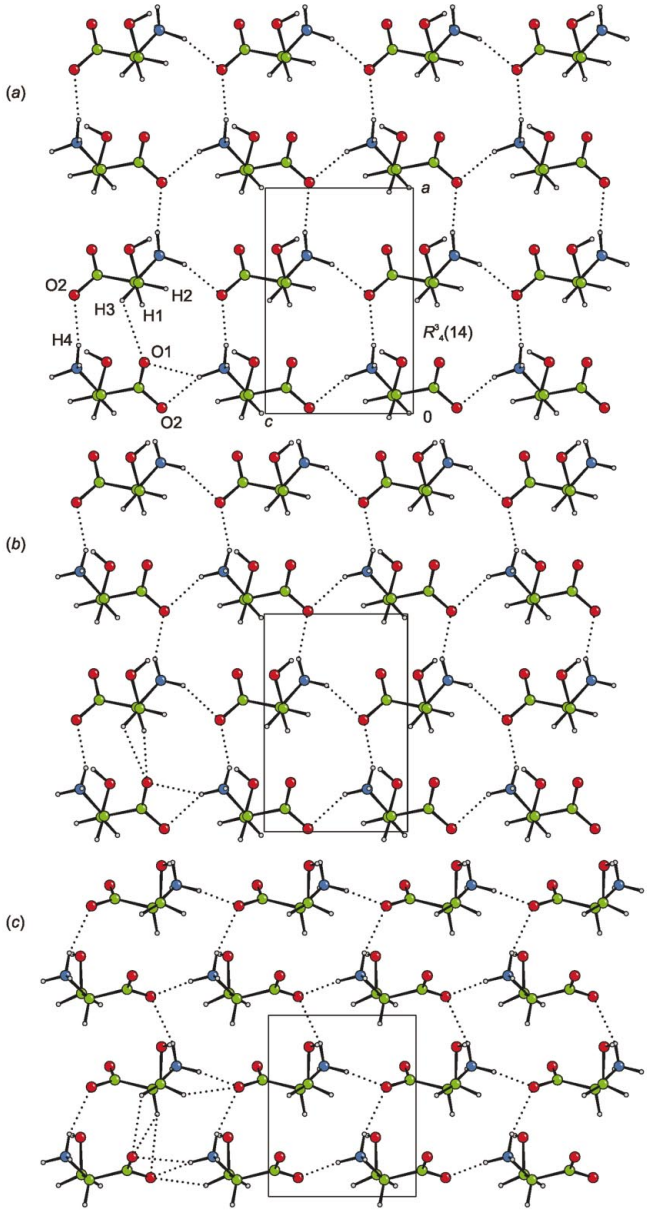

Figure 2
Effect of pressure on the crystal structure of L-serine as viewed along **b**: (*a*) L-serine-I at ambient pressure; (*b*) L-serine-I at 4.8 GPa; (*c*) L-serine-II at 5.4 GPa. This layer is referred to as the *B*-layer in the text. The orientations of all the diagrams are the same; the scale is the same as that used in Figs. 1 and 3. The bifurcation of the N1H5···O1/2 and CH···O bonding are shown only in the bottom-left fragment of the diagram. The colour scheme is as shown in Fig. 1.

The variation of hydrogen-bonding parameters in L-serine-I between 0.3 and 4.8 GPa is presented in Table 2. N1H4···O2 shortens from N···O 2.887 (4) Å at ambient pressure to 2.691 (13) Å at 4.8 GPa (Fig. 2*b*). A search of the Cambridge Database reveals that there are only three amino acid structures (out of 213) in which NH···O interactions are shorter than this, the shortest, 2.661 Å, being observed in L-arginine L-glutamate trihydrate (DUSMAF; Suresh *et al.*, 1986). The shortening of this distance occurs quite smoothly between 0.3 and 4.8 GPa. N1H6···O1 is formed approximately along the *b** axis (Fig. 1*b*) and reflection data along this direction of reciprocal space were severely shaded by the pressure cell. This distance is therefore not very precisely determined in the present study, but it also shortens from 2.840 (4) to 2.72 (3) Å.

The least compressible interaction is the head-to-tail, bifurcated, N1H5···O1/2 chain-forming interaction along **c**. The O···O interaction should just have one set which constitutes the three-centre hydrogen bond along this direction which decreases from O···O = 2.871 (3) to 2.775 (13) Å between ambient pressure and 4.8 GPa. The longer bond in this bifurcated motif decreases from 3.118 (3) to 2.981 (12) Å, which corresponds to an enhancement of the bifurcated character of this hydrogen bond. The crystal structure of α-glycine also contains head-to-tail chains of molecules and also in that structure an increase in bifurcation is also observed with pressure (Dawson *et al.*, 2005). The crystallographic direction parallel to this chain in α-glycine is the least compressible in the system (Boldyreva *et al.*, 2003), as it is here.

The hydrogen bonds in the OH···OH···OH chain formed by the side groups of the serine molecules are longer than those formed between the ammonium and carboxylate groups, and the O···O distances measure 2.918 (4) Å at ambient pressure. These interactions also decrease in length to 2.781 (11) Å. Brock & Duncan (1994) quote a range of 2.55–3.05 Å for the O···O distances in this type of interaction at ambient pressure, with an average of 2.79 (1) Å. The angles subtended at O3 in these chains increases from 148.5 (2)° at ambient pressure to 158.5 (7)° at 4.8 GPa.

We have recently described the crystal structure of α-glycine at 6.2 GPa (Dawson *et al.*, 2005). The structure consists of a stack of hydrogen-bonded bi-layers which interact *via* CH···O hydrogen bonds. Within the layers sets of $C(5)$ chains intersect to form $R^4_4(16)$ ring motifs. The effect of pressure was described in terms of the closing-up of holes in the middle of the $R^4_4(16)$ rings and the formation or shortening of CH . . . . ···O hydrogen bonds both across the $R^4_4(16)$ rings and between the bilayers. It is interesting to investigate whether

similar features can be observed in the compression of L-serine-I.

Inspection of space-filling plots (Fig. 6*a–f*) shows that there are holes in the centres of each of the $R_3^3(11)$, $R_3^3(13)$ and $R_3^4(14)$ ring motifs formed in L-serine-I. The shortening of the NH···O hydrogen bonds (even N1H4···O2, which became very short) is not enough to close up the holes in the middle of the $R_3^3(11)$ and $R_4^3(14)$ rings, which occur in the *A* and *B* layers, respectively. Closure of the hole in the centre of the $R_3^3(13)$ ring does occur though, and as this closure occurs along the *b*-axis direction, the greater compressibility of the *b* axis compared with the *a* and *c* axes is understandable. The closure occurs not only by a shortening of the O3···O3 distance from 2.918 (4) to 2.781 (11) Å, but also an increase in the O3···O3···O3 angles made along the chains of hydroxyl groups from 148.5 (2) to 158.5 (7)° (the angle made by the vector between the central O3 and the midpoint of the two flanking O3s and [010] is 15.4°; Fig. 1*b*). As these appear to be comparatively weak hydrogen bonds this is presumably a rather 'soft' parameter, which deforms easily under pressure.

CH···O interactions occur frequently in the structures of amino acids and in proteins (Desiraju & Steiner, 1999). A survey of amino-acid crystal structures determined by neutron diffraction showed that the most common H···O distances are around 2.4 Å, with a minimum of 2.15 Å (Jeffrey & Maluszynska, 1982). Generally, it is the H atom attached to the α-C atom which is involved in this type of interaction, as this is activated by the neighbouring ammonium and carboxylate groups (Derewenda *et al.*, 1995; Desiraju & Steiner, 1999); the H atoms of side chains are involved less frequently. L-Serine under ambient conditions does not conform to this general trend and under ambient conditions the strongest CH···O interactions are formed by the CH_2 group to the O atoms of neighbouring hydroxyl and carboxylate groups at normalized distances of 2.55 and 2.56 Å for C3H3···O1 and C3H2···O3, respectively. The shortest CH···O contact made by the αH atom is 2.75 Å at ambient pressure. CH···O hydrogen bonding from the C_αH group becomes more significant at high pressure and the normalized C2H1···O1 distance becomes 2.44 Å at 4.8 GPa. Most of the shortening in this interaction occurs between 0.3 and 2.9 GPa. The C3H3···O1 interaction shortens to 2.42 Å and together these interactions form a pair of contacts to the same O1 atom across the $R_4^3(14)$ rings in the *B* layers. These CH···O interactions can also be considered to support the N1H4···O1 interactions formed between the *A* layers.

Therefore, while the compression of α-glycine was characterized by the closing up of voids in *R* motifs with concomitant shortening of weak CH···O hydrogen bonds, that in L-serine-I is associated with the deformation and shortening of rather weak OH···OH hydrogen bonds. Although different interac-

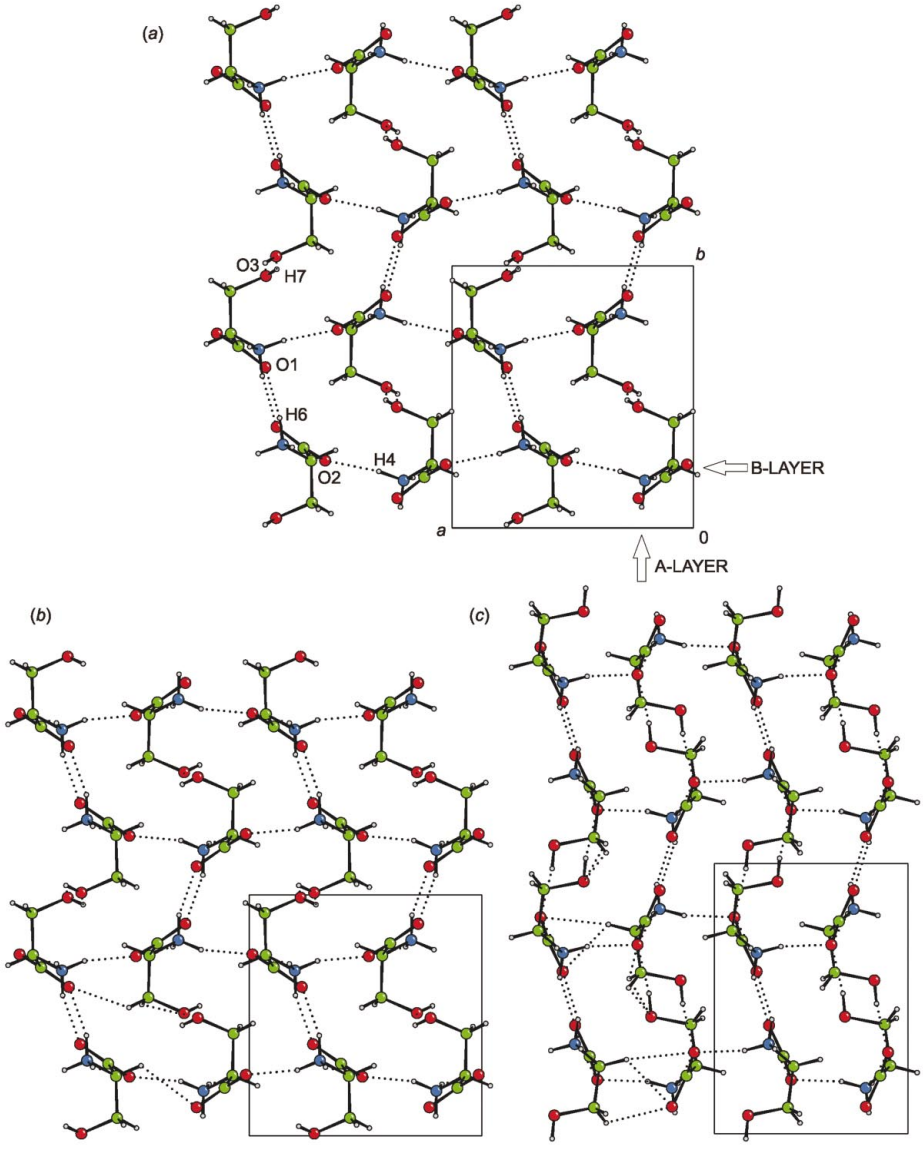

Figure 3
Effect of pressure on the crystal structure of L-serine as viewed along **c**: (*a*) L-serine-I at ambient pressure; (*b*) L-serine-I at 4.8 GPa; (*c*) L-serine-II at 5.4 GPa. The *A*-layers run vertically, the *B*-layers horizontally. The orientations of all diagrams are the same; the scale is the same as that used in Figs. 1 and 2. The CH···O bonding is shown only in the bottom-left fragment of the diagram. Colour scheme: as shown in Fig. 1.

Table 2
Hydrogen-bonding parameters (Å, °) in L-serine-I.

The distances to hydrogen have been normalized to neutron values (see §2.2).

Pressure (GPa)	0	0.3	1.4	2.9	4.1	4.8
N1H5···O2^{i}						
H5···O2	1.91	1.94	1.89	1.86	1.86	1.86
N1···O2	2.871 (3)	2.862 (15)	2.814 (14)	2.786 (12)	2.775 (12)	2.775 (13)
∠N1H5O2	158 (2)	153	152	153	150	150
N1H5···O1^{i}						
H5···O1	2.29	2.30	2.28	2.24	2.22	2.19
N1···O1	3.118 (3)	3.106 (15)	3.070 (14)	3.028 (11)	3.010 (12)	2.981 (12)
∠N1H5O1	139 (2)	138	136	136	136	136
N1H4···O2^{ii}						
H4···O2	1.90	1.89	1.86	1.82	1.80	1.78
N1···O2	2.887 (4)	2.825 (16)	2.796 (15)	2.751 (12)	2.709 (13)	2.691 (13)
∠N1H4O2	167 (2)	153	153	153	150	149
N1H6···O1^{iii}						
H6···O1	1.87	1.86	1.81	1.80	1.79	1.76
N1···O1	2.840 (4)	2.81 (3)	2.76 (3)	2.75 (2)	2.75 (3)	2.72 (3)
∠N1H6O1	162 (2)	158	157	157	159	158
O3H7···O3^{iv}						
H7···O3	2.02	1.98	1.98	2.00	1.92	2.08
O3···O3	2.918 (4)	2.882 (16)	2.842 (14)	2.807 (12)	2.790 (12)	2.781 (11)
∠O3H7O3	153 (3)	153 (14)	147 (7)	139 (6)	147 (6)	129 (7)
∠O3···O3···O3	148.5 (2)	151.2 (14)	155.4 (12)	158.1 (8)	158.9 (7)	158.5 (7)
C2H1···O1^{v}						
H1···O1	2.75	2.67	2.56	2.48	2.45	2.44
C2···O1	3.368 (4)	3.307 (16)	3.222 (15)	3.153 (13)	3.113 (13)	3.106 (13)
∠C2H1O1	118.3(13)	118	120	121	120	120
C3H2···O3^{iv}						
H2···O1	2.56	2.57	2.54	2.51	2.50	2.48
C3···O1	3.214 (4)	3.182 (17)	3.147 (16)	3.099 (14)	3.076 (13)	3.062 (13)
∠C3H2O3	117.6 (12)	116	116	115	114	114
C3H3···O1^{v}						
H2···O1	2.55	2.48	2.46	2.44	2.43	2.42
C3···O1	3.053 (4)	3.005 (14)	2.942 (13)	2.905 (11)	2.876 (11)	2.871 (11)
∠C3H3O1	109.4 (18)	110	107	107	105	105

Symmetry codes: (i) $x, y, 1+z$; (ii) $\frac{1}{2}+x, \frac{1}{2}-y, -z$; (iii) $\frac{1}{2}-x, -y, \frac{1}{2}+z$; (iv) $\frac{1}{2}-x, 1-y, \frac{1}{2}+z$; (v) $-\frac{1}{2}+x, \frac{1}{2}-y, -z$.

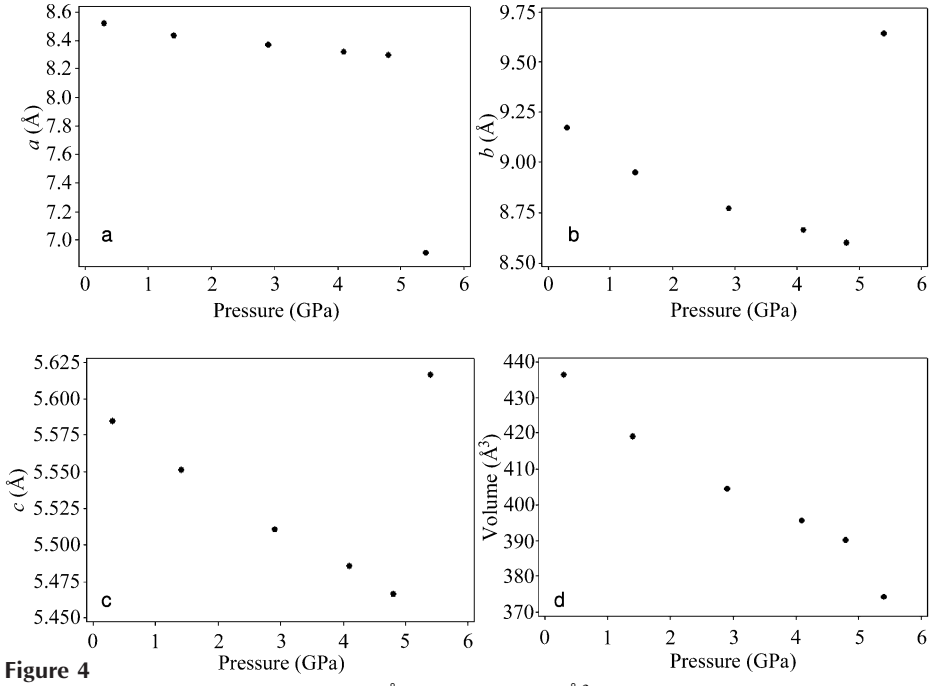

Figure 4
Variation of the lattice parameters (*a*–*c*, Å) and volume (*d*, Å^3) of L-serine as a function of pressure (GPa).

tions are involved in the two amino acids, both might be considered easily deformable. The formation of CH···O hydrogen bonds between the layers in the α-glycine structure is paralleled in L-serine-I by CH···O bond formation between the *A* layers (Fig. 3*b*).

One interesting conclusion of the, admittedly limited, research that has been carried out on hydrogen-bonded molecular systems is that super-short hydrogen bonds are not formed by the application of pressures below *ca* 10 GPa. The lower distance limits for such interactions which apply at ambient pressure also seem to apply at high pressure. In serine at 4.8 GPa at least one N···O distance (N1H4···O2) approaches the lower limit for this kind of interaction observed in the Cambridge Database. Above this pressure a phase change occurs to a hitherto uncharacterized phase, L-serine-II.

3.3. L-Serine-II at 5.4 GPa

The transition from L-serine-I to L-serine-II occurs with a marked reduction in the volume of the unit cell (Fig. 4). The volume per non-H atom in phase II is only 13.4 Å^3. Remarkably, the transition proceeds from one single crystal of L-serine-I to a single crystal of L-serine-II, and this transition is fully reversible.

The observation that this transition occurs from one single crystal to another strongly implies that the overall topologies of phases I and II are similar to each other. This proves to be the case, and the structure also consists of two sets of layers which are stacked along the *a* and *b* directions (Figs. 1*c* and 2*c*; hydrogen-bonding information is presented in Table 3). In terms of hydrogen bonds formed, the structure of the *B* layers is the same as in L-serine-I. Chains are formed by lattice repeats along **c** in which the molecules interact *via* three-centre N1H5···O1/2 bonds. In a reversal of the trend established during the compression of L-serine-I, these bonds are less symmetrical than the equivalent ones in L-serine-I at 4.8 GPa.

Neighbouring chains are linked into a *B*-layer by N1H4···O2 hydrogen bonds, to build $R_4^3(14)$ motifs (Fig. 2*c*). These are completely analogous to those in the *B*-layers of L-serine-I, but the rings in L-serine-II are longer and thinner (*cf.* Figs. 2*a*–*c*). This change occurs by

Table 3
Table of hydrogen-bonding parameters (Å, °) for L-serine-II at 54 GPa.

H-atom coordinates have been normalized to neutron values.

	H···*A*	*D*···*A*	∠*D*—H···*A*
N1H5···O2^{i}	1.86	2.810 (14)	155
N1H5···O1^{i}	2.30	3.145 (11)	141
N1H4···O2^{ii}	1.89	2.850 (10)	159
N1H6···O1^{iii}	1.76	2.64 (2)	143
O3H7···O2^{iii}	1.71	2.62 (2)	152
C2H1···O1^{v}	2.50	3.059 (13)	111
C2H1···O2^{v}	2.37	3.411 (10)	162
C3H2···O2^{i}	2.40	3.149 (13)	125
C3H2···O3^{iv}	2.45	3.276 (15)	132
C3H3···O3^{vi}	2.37	3.207 (15)	133
C3H3···O1^{v}	2.42	2.982 (10)	111

Symmetry codes: (i) $x, y, 1+z$; (ii) $-\frac{1}{2}+x, \frac{1}{2}-y, -z$; (iii) $\frac{1}{2}+x, \frac{1}{2}-y, -z$; (iv) $\frac{1}{2}-x, -y, \frac{1}{2}+z$; (v) $\frac{1}{2}-x, 1-y, \frac{1}{2}+z$; (vi) $\frac{1}{2}-x, 1-y, -\frac{1}{2}2+z$.

(i) opposite displacements of the molecules in successive N1H5···O2 chains along the *c* direction (*i.e.* the chains slide across each other), and

(ii) compression of the distance between the chains along the *a* direction.

Thse changes enable compression of the $R_4^3(14)$ rings without further shortening the N1H4···O1 hydrogen bond. Inspection of the space-filling plots shows that the voids which occur in the centre of the $R_4^3(14)$ rings in L-serine-I even at 4.8 GPa close up during the phase transition (*cf.* Figs. 6*c*, *f* and *i*). The dimensions of the ring are equal to *a*/2 and *c*, and so the transition effects the lengths of the *a* and *c* unit-cell axes, the former sharply decreasing and the latter increasing slightly relative to L-serine-I.

As in L-serine-I, the structure of the *A*-layers consists of ribbons in which *C*(5) chains formed by N1H5···O2 hydrogen bonds are linked by N1H6···O1 hydrogen bonds (Fig. 1*c*). The N1···O1 distances $R_3^3(11)$ rings so-formed appear to be somewhat shorter than in L-serine-I at 4.8 GPa, although the standard uncertainties are high. There is a substantial change in the way the ribbons are connected into a layer. In L-serine-I this was achieved through OH···OH interactions, but in L-serine-II these are replaced by much stronger O3H7···O2 hydroxyl to carboxylate hydrogen bonds. This generates $R_3^2(13)$ motifs which replace the $R_3^3(13)$ motifs. The hydroxyl H7 atom was located in a difference-Fourier map and is clearly attached primarily to O3. Its position was also optimized in a plane-wave DFT calculation, with results consistent with those implied by the difference map (details of these calculations will be described in another publication). The length of the new hydrogen bond is very short, with an O3···O2 distance of 2.62 (2) Å, although the (normalized) H7 . . . . . O2 distance is 1.71 Å. In order to accommodate this interaction the N1—C2—C1—O2 torsion angle changes from −178.1 (2)° at 4.8 GPa to −156.3 (10)° at 5.4 GPa. The orientation of the O3H7 group changes from being *gauche* to *anti* with respect to C2—C3. This movement of the H atom implies that the *C*(5) chains which run along **c** must move apart slightly, with the result that the *b* axis is actually *ca* 0.5 Å longer in L-serine-II than in L-serine-I.

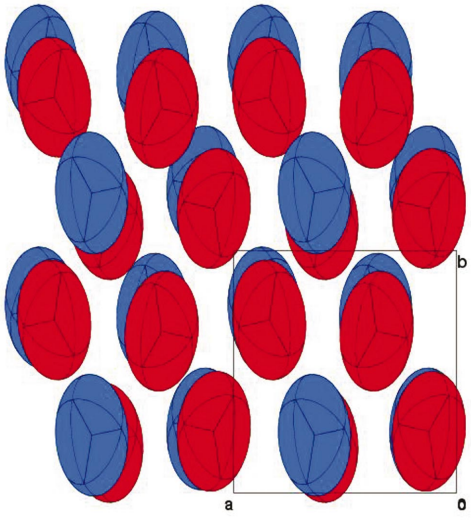

Figure 5
Comparison of packing in the structures of L-serine-I at ambient pressure (blue) and 4.8 GPa (red). Molecules are represented by their inertial tensor ellipsoids. The unit cell shown corresponds to the ambient pressure phase. Note that the molecules do not greatly change orientation.

The formation of L-serine-II is also characterized by a marked increase in CH···O hydrogen bonding, with each H atom making two interactions. These occur within the *A*-layers between the CH_2 groups and the hydroxyl and carboxylate groups of neighbouring molecules involved in the new $R_3^2(13)$ ring motifs. In the *B*-layers they are formed across the $R_4^3(14)$ rings in the direction of the *a* axis; they can therefore be considered to stabilize the compression of these rings.

4. Conclusions

We have described the effect of high pressure on the crystal structure of L-serine. The structure can be considered to consist of two sets of layers, which stack along the *a* and *b* axes of the unit cell, and which have been referred to above as the *A*- and *B*-layers. The *A*-layers contain NH···O and OH . . . . . OH interactions which combine to give $R_3^3(11)$ and $R_3^3(13)$ ring motifs; NH···O interactions in the *B*-layers form $R_4^3(14)$. The $R_3^4(14)$ motifs within the *B*-layers can also be viewed as connections between the *A*-layers. This structure remains stable up to 4.8 GPa. It undergoes anisotropic compression in which the principal structural effect is to compress voids in the middle of the $R_3^3(13)$ rings of the *A*-layers by deforming the rather 'soft' hydrogen-bonded hydroxyl chains. The stacking distance between the *A*-layers also decreased, with a shortening of NH···O hydrogen bonds supported by the formation of CH···O hydrogen bonds. This latter effect continued until, at 4.8 GPa, the length of the NH···O hydrogen bonds approached the minimum value observed for this kind of interaction. Above 4.8 GPa a single-crystal-to-single-crystal phase change to L-serine-II occurs.

The phase change from L-serine-I to L-serine-II is accomplished by the change in two torsion angles and small positional displacements, and there are no major changes in the orientations of the molecules. The observation that the

transformation occurs from one single crystalline form to another is therefore readily understood. In the new phase the hydrogen-bonded links in the *A*-layers between OH···OH groups are replaced by stronger, shorter OH···carboxyl interactions. The layers also move closer together by closing-up voids which occur in the centres of the $R_4^3(14)$ rings. All three H atoms which are attached to carbon take part in two CH···O interactions. The *b* and *c* axes are longer in L-serine-II than in L-serine-I, but the *a* axis is substantially shorter and the overall effect is a reduction in the volume of the unit cell. This reduction is ascribable to the closing-up of the voids in the $R_4^3(14)$ rings.

In L-serine high pressure closes up voids which occur in *R* motifs and decreases the interactions between layers by CH···O hydrogen-bond formation. Similar comments apply to the behaviour of glycine under pressure. We are currently investigating the effect of pressure on other α-amino acids and it will be interesting to discover to what extent these same effects apply in those systems.

We thank the EPSRC for funding and The Cambridge Crystallographic Data Centre and Professor W. I. F. David (ISIS Facility, Rutherford Appleton Laboratory) for a copy of the program *DASH* which is able to accept single-crystal diffraction data.

References

Allan, D. R. & Clark, S. J. (1999). *Phys. Rev. B*, **60**, 6328–6334.

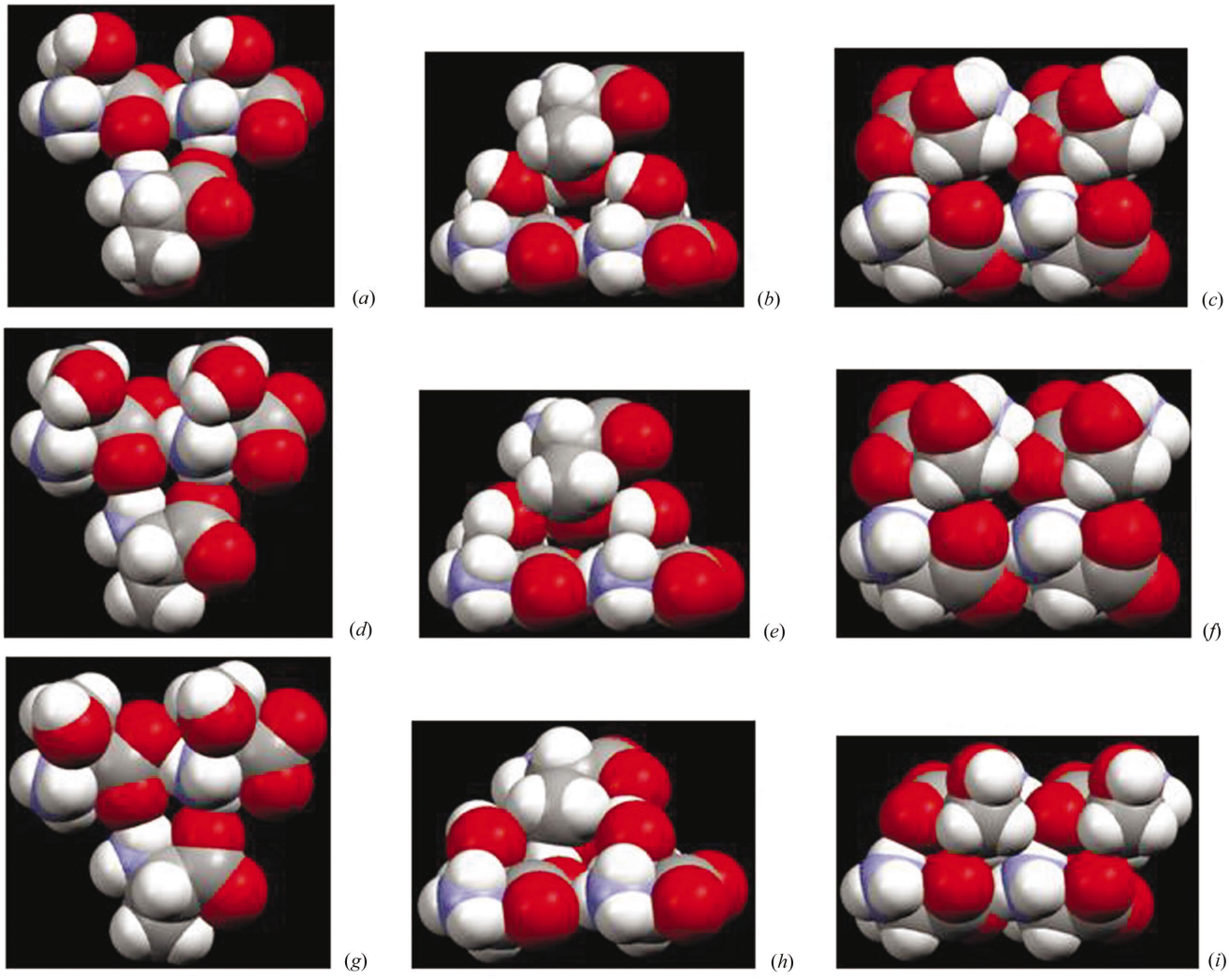

Figure 6
Space-filling plots showing *R*-type graph sets which occur in L-serine phases I and II as a function of pressure. The top, middle and bottom rows correspond to the L-serine-I at ambient pressure, L-serine-I at 4.8 GPa and L-serine-II at 5.4 GPa, respectively. On the left of the diagram (*a*), (*d*) and (*g*) are all $R_3^3(11)$ motifs which occur in the *A*-layers (*cf.* Fig. 1); the hole in this small ring does not become very much smaller with increasing pressure. In the middle column of the diagram (*b*) and (*e*) show $R^3{}_3(13)$ motifs, which also occur in the *A*-layers (*cf.* Fig. 1). Note that the hole in the middle of the ring is significantly smaller at 4.8 GPa than at ambient pressure. At 5.4 GPa (*h*) the $R_3^3(13)$ motif of form I has been converted into $R_3^2(13)$ in form II. On the right of the figure (*c*), (*f*) and (*i*) show the $R_4^3(14)$ rings. Although the hole in the middle of this ring does not close-up in form I between ambient (*c*) and 4.8 GPa (*f*), it does in L-serine-II at 5.4 GPa (*i*).

Allan, D. R., Clark, S. J., Brugmans, M. J. P., Ackland, G. J. & Vos, W. L. (1998). *Phys. Rev. B*, **58**, R11809–R11812.
Allan, D. R., Clark, S. J., Dawson, A., McGregor, P. A. & Parsons, S. (2002). *Acta Cryst.* B**58**, 1018–1024.
Allan, D. R., Clark, S. J., Ibberson, R. M., Parsons, S., Pulham, C. R. & Sawyer, L. (1999). *Chem. Commun.* pp. 751–752.
Allan, D. R., Clark, S. J., Parsons, S. & Ruf, M. (2000). *J. Phys. Condensed Matter*, **12**, L613–L620.
Allan, D. R., Parsons, S. & Teat, S. J. (2001). *J. Synchrotron Rad.* **8**, 10–17.
Allen, F. H. (2002). *Acta Cryst.* B**58**, 380–388.
Allen, F. H. & Motherwell, W. D. S. (2002). *Acta Cryst.* B**58**, 407–422.
Benedetti, E., Pedone, C. & Sirigu, A. (1973). *Gazz. Chim. Ital.* **103**, 555–561.
Bernstein, J., Davis, R. E., Shimoni, L. & Chang, N.-L. (1995). *Angew. Chem. Int. Ed. Engl.* **34**, 1555–1573.
Betteridge, P. W., Carruthers, J. R., Cooper, R. I., Prout, K. & Watkin, D. J. (2003). *J. Appl. Cryst.* **36**, 1487.
Boldyreva, E. V. (2003). *J. Mol. Struct.* **647**, 159–179.
Boldyreva, E. V. (2004*a*). *J. Mol. Struct.* **700**, 151–155.
Boldyreva, E. V. (2004*b*). *Cryst. Engng*, **6**, 235–254.
Boldyreva, E. V. (2004*c*). *NATO Science Series, II: Mathematics, Physics & Chemistry*, edited by A. Katrusiak & P. F. McMillan, Vol. 140, pp. 495–512. Dordrecht: Kluwer Academic Publishers.
Boldyreva, E. V., Ahsbahs, H. & Weber, H.-P. (2003). *Z. Kristallogr.* **218**, 231–236.
Boldyreva, E. V., Ivashevskaya, S. N., Sowa, H., Ahsbahs, H. & Weber, H.-P. (2004). *Doklady Phys. Chem.* **396**, 358–361.
Boldyreva, E. V., Naumov D. Yu. & Ahsbahs, H. (1998). *Acta Cryst.* B**54**, 798–808.
Brock, C. P. & Duncan, L. L. (1994). *Chem. Mater.* **6**, 1307–1312.
Bruker AXS (2003). *SAINT*, Version 7. Bruker-AXS, Madison, Wisconsin, USA.
Bruno, I. J., Cole, J. C., Edgington, P. R., Kessler, M., Macrae, C. F., McCabe, P., Pearson, J. & Taylor, R. (2002). *Acta Cryst.* B**58**, 389–397.
David, W. I. F., Shankland, K., Cole, J., Maginn, S., Motherwell, W. D. S. & Taylor, R. (2001). *DASH User's Manual.* Cambridge Crystallographic Data Centre, Cambridge, UK.
Dawson, A., Allan, D. R., Belmonte, S. A., Clark, S. J., David, W. I. F., McGregor, P. A., Parsons, S., Pulham, C. R. & Sawyer, L. (2005). Accepted for publication.
Dawson, A., Allan, D. R., Clark, S. J., Parsons, S. & Ruf, M. (2004). *J. Appl. Cryst.* **37**, 410–416.
Derewenda, Z. S., Lee, L. & Derewenda, U. (1995). *J. Mol. Biol.* **252**, 248–262.
Desiraju, G. R. & Steiner, T. (1999). *The Weak Hydrogen Bond.* IUCr Monographs on Crystallography No. 9. Oxford University Press, Oxford, UK.
Farrugia, L. J. (1999). *J. Appl. Cryst.* **32**, 837–838.
Hemley, R. J. & Dera, P. (2000). *Rev. Mineral. Geochem.* **41**, 335–419.
Jeffrey, G. A. & Maluszynska, H. (1982). *Int. J. Biol. Macromol.* **4**, 173–185.
Katrusiak, A. (2004). *NATO Science Series, II: Mathematics, Physics and Chemistry*, edited by A. Katrusiak & P. F. McMillan, Vol. 140, pp. 513–520. Dordrecht: Kluwer Academic Publishers.
Kistenmacher, T. J., Rand, G. A. & Marsh, R. E. (1974). *Acta Cryst.* B**30**, 2573–2578.
Larson, A. C. (1970). *Crystallogr. Comput. Proc. Int. Summer Sch.* pp. 291–294.
Merrill, L. & Bassett, W. A. (1974). *Rev. Sci. Instrum.* **45**, 290–294.
Parsons, S. (2004). *SHADE.* The University of Edinburgh, Scotland.
Sheldrick, G. M. (1997). *SHELXL*97. University of Göttingen, Germany.
Sheldrick, G. M. (2004). *SADABS.* Bruker-AXS, Madison, Wisconsin, USA.
Spek, A. L. (2004). *PLATON.* Utrecht University, The Netherlands.
Suresh, C. G., Ramaswamy, J. & Vijayan, M. (1986). *Acta Cryst.* B**42**, 473–478.
Watkin, D. J., Pearce, L. & Prout, C. K. (1993). *CAMERON.* Chemical Crystallography Laboratory, University of Oxford, England.